Title

The genome of a bunyavirus cannot be defined at the level of the viral particle but only at the scale of the viral population.

Journal

Proceedings of the National Academy of Sciences, 120(48)

Authors

Dasgupta, Ranjit

Parker, Maxwell

Ben-Mahmoud, Sulley

et al.

Publication Date

2023-11-28

DOI

10.1073/pnas.2309412120

Peer reviewed

PNAS RESEARCH ARTICLE | MICROBIOLOGY

The genome of a bunyavirus cannot be defined at the level of the viral particle but only at the scale of the viral population

Michel Yvon[a], Thomas L. German[b], Diane E. Ullman[c], Ranjit Dasgupta[b], Maxwell H. Parker[b], Sulley Ben-Mahmoud[c], Eric Verdin[d], Patrick Gognalons[d], Aurélie Ancelin[e], Joséphine Laï Kee Him[e], Justine Girard[e], Marie-Stéphanie Vernerey[a], Emmanuel Fernandez[a], Denis Filloux[a], Philippe Roumagnac[a], Patrick Bron[e], Yannis Michalakis[f,1], and Stéphane Blanc[a,1,2]

Edited by Esteban Domingo, Spanish National Research Council, Madrid, Spain; received June 11, 2023; accepted October 21, 2023

Bunyaviruses are enveloped negative or ambisense single-stranded RNA viruses with a genome divided into several segments. The canonical view depicts each viral particle packaging one copy of each genomic segment in one polarity named the viral strand. Several opposing observations revealed nonequal ratios of the segments, uneven number of segments per virion, and even packaging of viral complementary strands. Unfortunately, these observations result from studies often addressing other questions, on distinct viral species, and not using accurate quantitative methods. Hence, what RNA segments and strands are packaged as the genome of any bunyavirus remains largely ambiguous. We addressed this issue by first investigating the virion size distribution and RNA content in populations of the tomato spotted wilt virus (TSWV) using microscopy and tomography. These revealed heterogeneity in viral particle volume and amount of RNA content, with a surprising lack of correlation between the two. Then, the ratios of all genomic segments and strands were established using RNA sequencing and qRT-PCR. Within virions, both plus and minus strands (but no mRNA) are packaged for each of the three L, M, and S segments, in reproducible nonequimolar proportions determined by those in total cell extracts. These results show that virions differ in their genomic content but together build up a highly reproducible genetic composition of the viral population. This resembles the genome formula described for multipartite viruses, with which some species of the order *Bunyavirales* may share some aspects of the way of life, particularly emerging properties at a supravirion scale.

Bunyavirales | orthotospovirus | genome packaging | multipartite virus | genome formula

Significance

Bunyaviruses infect animals, plants, fungi, and protists. Despite their importance, fundamental aspects of their biology as basic as the definition of their genome remain elusive. The viral genome consists of several negative or ambisense RNA segments, and virions often miss segments and/or package complementary strands. We formally quantify this heterogeneity on the species *Tomato spotted wilt orthotospovirus*. Within individual virus particles, the number, the identity, and the polarity of the segments are widely variable. In contrast, we show that a stable genetic composition is an emerging property of the viral population, each of the RNA segments/polarities accumulating reproducibly at a specific frequency. This resembles the genome formula of multipartite viruses, suggesting that bunyaviruses may also function as multicomponent viral systems.

The order *Bunyavirales* was established by the ICTV to contain viral species with two to eight single-stranded RNA genomic components with negative (sequence complementary to coding strand) or ambisense (coding in both orientations) polarity (1, 2). The order is divided into 14 families that include nearly 500 virus species infecting vertebrates, invertebrates, plants, fungi, and protists (2, 3). Many of the well-characterized member species of this order are considered emerging viruses and cause serious diseases impacting human health and agriculture productivity globally (4, 5). Except for the family *Hantaviridae*, all bunyaviruses infecting animals and plants are transmitted by insect or tick vectors in which the virus can also replicate, complicating efforts to control disease spread.

Despite the importance of this viral order, some very basic aspects of the biology of the most important species remain mysterious. To illustrate this statement, one can consider the very simple question of what the genome of these viruses is, i.e., what is effectively packaged and transmitted to new hosts. The canonical view describes the production of membrane-bound glycoproteins that together delineate a spherical particle. Each particle is considered to enclose one of each of the negative or ambisense RNA segments. Packaged together, these segments constitute the complete genome that is transmitted to a new host, putatively as a "one is enough" particle. The current terminology resulting from these assumptions describes the virion contained RNAs as viral sense (vRNAs), and the unencapsidated complementary RNAs generated during genome replication as viral complementary sense (vcRNAs). The literature, including the most prominent Virology web sites, is replete with cartoons depicting packaged genomic segments of vRNA complexed with the N protein that interacts with the inner domain of the glycoproteins associated with the membrane (for example, see refs. 6 and 7). A few copies of the polymerase, the L protein, are also shown to be associated with the genomic RNA segments within particles, as this protein is required for transcription of negative vRNA strands prior to protein production.

Many experimental findings contradict this dogma (8). First, the viral particles have been reported to be of highly variable size (9, 10) and, in the case of Lacrosse virus (LACV), this particle size variation has been speculated to correlate with RNA content

The authors declare no competing interest.

This article is a PNAS Direct Submission.

[1]Y.M. and S.B. contributed equally to this work.

[2]To whom correspondence may be addressed. Email: stephane.blanc@inrae.fr.

This article contains supporting information online at https://www.pnas.org/lookup/suppl/doi:10.1073/pnas.2309412120/-/DCSupplemental.

Published November 20, 2023.

variation (9). Second, some semi-quantitative observations of the relative amounts of the distinct RNA segments in purified virus particles of different *Bunyavirales* species have indicated that they are not equi-molar (11–17), ruling out a presumed efficient packaging of exactly one copy of each segment per virion. Third, in numerous instances such as tomato spotted wilt virus (13) (TSWV), Uukuniemi virus (18) (UUKV), and rift valley fever virus (15, 19) (RVFV), viral complementary sense strands of the S and M RNAs have been convincingly detected within virions, though in low amount not formally quantified. Whether the encapsidation of the vcRNAs is functionally relevant or whether it is an exception or the rule in the order *Bunyavirales* is thus far unclear. Fourth, the possibility of packaging some viral mRNA has been envisaged (13, 15), though experimental evidence appears to plead against it. Finally, the identity of RNA segments and their number within individual virus particles of RVFV has been directly studied via an elegant single molecule in situ hybridization approach (15, 17). Distinguishing between vRNAs and vcRNAs polarities (15) or not (17), these two seminal studies very convincingly showed, for the first time with a direct approach, that virions differ in their RNA content, some missing segments, whereas others have extra copies (20), and that the majority of virus particles within a population are not able to express the complete viral genetic information. It is interesting to note that the same studies demonstrated that particles containing incomplete segment sets are nevertheless capable of entering host cells; hence, they could putatively have a functional role through complementation. Consistent with this, earlier papers described genetic engineering of artificial segments of UUKV that could not ensure the complete replication cycle but were nevertheless packaged and possibly transmitted to neighboring cells (21, 22). Thus, despite considerable evidence that the packaging of genome segments of bunyaviruses is highly heterogeneous, which RNA species are packaged (segment and polarity), in what proportions, whether these proportions are reproducible at the virus population level, and whether the packaging process is nonspecific are still open questions that have never been formally and quantitatively addressed together on a single species.

Here, using the plant infecting TSWV, we explore these questions with several complementary quantitative approaches. With few variations, the molecular biology of TSWV is similar to many member species of the order *Bunyavirales* infecting animals (5), with three segments (L, M, and S) of negative (L) or ambisense polarity (M and S). Using (cryo)electron microscopy and tomography, we establish the virus particle size distribution. We further characterize the amount of RNA content of viral particles and demonstrate that RNA content and particle size do not correlate. Using Nanopore direct RNA sequencing, we show that both vRNAs and vcRNAs of all three genomic segments are packaged, though in different proportions depending on the segments. In contrast, messenger RNAs are not packaged, not even in minute amounts. The development of a strand-specific Reverse Transcription (RT) qPCR protocol allowed us to thoroughly quantify the number of copies of each segment and polarity in a large number of samples, indicating that each RNA species is packaged in very reproducible proportions across infected plants thereby defining a "genome formula" at the population level. Finally, the genome formula obtained from infected plant total extracts is very similar to that obtained from virus particles isolated from these extracts, formally supporting a nonspecific packaging process where all "available" viral genomic RNAs, of both polarities, are packaged with the same efficiency. Together, by demonstrating that the genome is not recapitulated in individual but in a population of virions, our results highlight important issues of the biology of bunyaviruses, at least of TSWV, that are reminiscent of the biology of multipartite viruses.

Results

Virus Particle Size and RNA Content Are Highly Variable and Do Not Correlate. To accurately estimate the diameter of TSWV virions, we recorded cryoelectron microscopy (cryo-EM) images of the frozen-hydrated purified virus preparation (Fig. 1*A*). With this observation method, the sample is immediately frozen/vitrified in a cryogenic liquid and imaged at very low temperature, avoiding distortion of the morphology of biological objects. From cryo-EM images, we estimated the diameter of 4861 purified TSWV particles, which appear as near-perfect spheres. The large number of analyzed virions confirmed an important heterogeneity in diameter that ranges from 65 to 135 nm, unimodally and near-symmetrically distributed around an average of ~100 nm (Fig. 1*B*). From the diameter, the estimated volume of the spherical TSWV particles ranges from 1.44×10^{-10} to 1.29×10^{-9} nL, thus an impressive volume difference close to one order of magnitude.

When observing semi-thin sections of TSWV particles fixed and embedded into a classical electron microscopy resin (Fig. 1*C*), not only did we consistently observe the heterogeneity of their diameter but, interestingly, also of their inner densities which most likely represent ribonucleoprotein (RNP) segments (*SI Appendix*, Fig. S1 and Movie S1). Tomographic analysis allowed the 3D reconstruction of the volumes corresponding to these inner densities (Fig. 1 *C*3 and *C*4). Remarkably, virus particles could contain 1, 2, 3, or 4 discrete volumes. We relegate arguments on whether each volume represents a distinct segment or not to the *Discussion*.

Summing up all volumes of the inner density within a given virus particle provides an estimate of the amount of packaged RNPs. We extracted tomograms from 25 randomly chosen particles with the only constraint that they are entirely embedded in the resin (not cut through by the section) and plotted their diameter against the calculated total inner density volume. Particle size and the amount of encapsidated genetic material are not correlated (Fig. 1*D*).

Direct Nanopore RNA Sequencing Reveals the Packaging of Both Viral and Complementary Strands for the Three Genomic Segments but Not of Messenger RNAs. After demonstrating the huge variation in the volume of packaged genetic material within individual virions (fourfold to fivefold variation in Fig. 1*D*), we further explored the potential heterogeneity in the identity/nature of RNAs. In other words, which viral RNA species (identity and polarity of viral segments, viral mRNA) could be packaged in virions and in what proportion? We purified virus particles from a single infected plant and extracted the viral RNA. Direct Nanopore RNA sequencing was performed as indicated in the *Materials and Methods* (row data set is available at https://www.ncbi.nlm.nih.gov/sra/PRJNA1020112) and all viral reads, either of viral or complementary polarity, were mapped to the sequence of S, M, and L segments of TSWV isolate MR-01 (Fig. 2*A*). According to this technology (23, 24), sequencing is always initiated at the 3′ extremity of the RNA and proceeds toward the 5′ extremity with an efficiency that decreases with length, i.e., the reads can be stopped for many uncontrolled reasons at any time and so regions lying further from the 3′ end have less chance to be reached in a given read. We further calculated the sequencing depth that illustrates the number of times a given nucleotide of the RNAs has been read in an experiment, and doing so, we could obtain a quantitative estimate as described in the *Materials and Methods* and as further

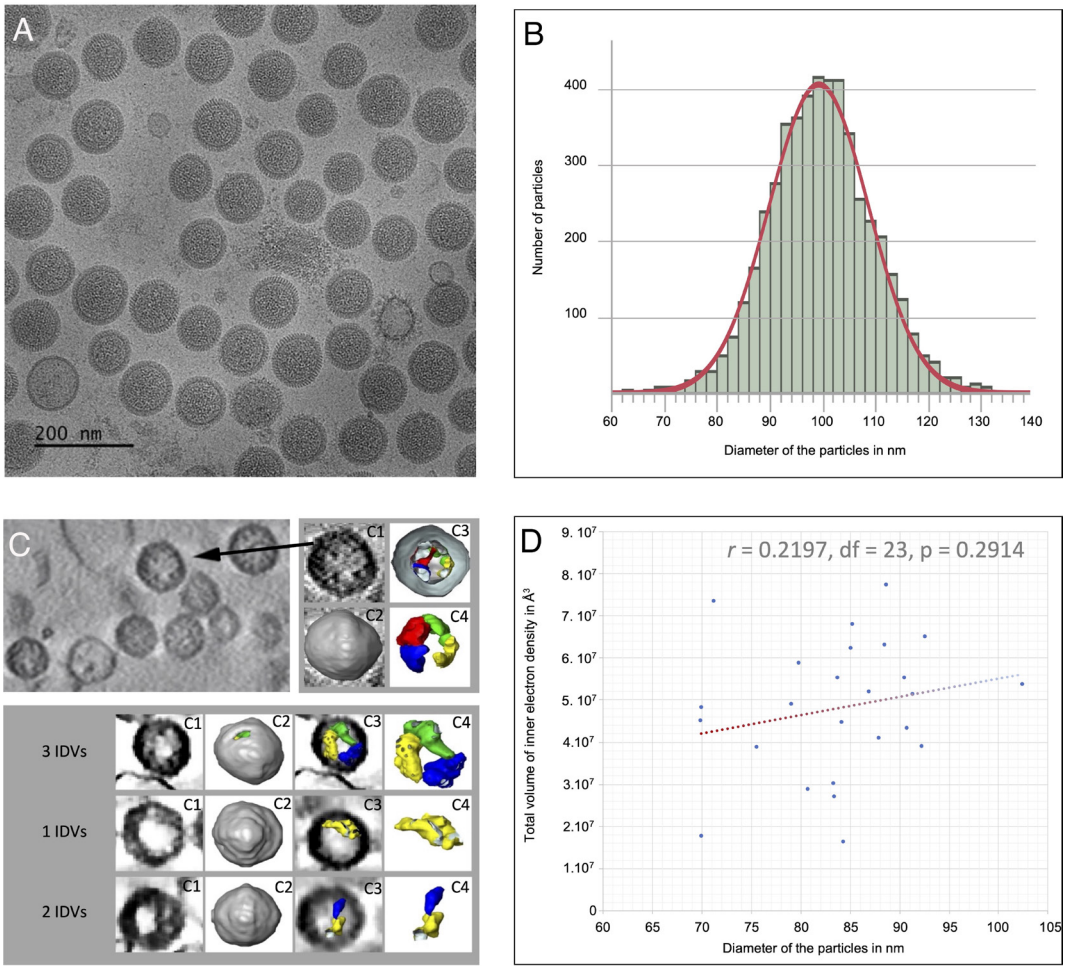

Fig. 1. Particles of TSWV are highly heterogeneous in size and RNA content. (*A*) Cryo-EM image of frozen-hydrated purified virus particles. (*B*) Histogram of the diameter distribution of virus particles, n = 4,861. The red line illustrates the best fit to a normal distribution. Although not passing the Kolmogorov–Smirnov test (*P*-value = 0.035), because of very slight over-representation of large and under-representation of small values, the distribution is unimodal and approximately symmetrical around the average of 100 nm. This histogram results from two independent virion preparations where the diameter of 1,964 and 2,897 particles was respectively estimated. (*C*) Electron tomography and segmentation of virus particles embedded in resin and semi-thin sectioned. The arrow indicates one reconstituted virus particle visible in the semi-thin section. The other particles, each constituting one line of the lower panel, were chosen from other regions of the semi-thin section. Micrographs labeled *C*1: Central section of the electron tomogram reconstruction of a complete viral particle. Micrographs labeled *C*2, *C*3, and *C*4 are different representations of the segmentation of 3D reconstructions of viral particles. *C*2 shows the surface of reconstructed virus particles, and *C*3 combines the central section of the viral particles with the segmentation of their inner density volumes (IDV) which are isolated and slightly magnified in *C*4. Extensive views of viral particles from the semi-thin section in *C* are presented as *SI Appendix*, Fig. S1 and Movie S1. (*D*) Analysis of the relationship between the diameter of the particles and the total volume of their inner density (the latter most likely corresponding to packaged ribonucleoproteins). Pearson's correlation coefficient (at the top) is low, and a linear regression is not statistically significant indicating an absence of correlation.

considered in the *Discussion*. The trends within this sample and with this technique were: i) when summing both polarities RNA-L appeared as the least accumulated (~1,200 copies for which the sequencing was initiated), RNA-M was slightly more frequent (~2,200 copies) and RNA-S clearly dominated (~11,000 copies); ii) contrary to the canonical view outlined in the introductory paragraphs, the viral complementary polarity can be highly represented in packaged RNA. While the vcRNA-L is rare and appears here as 3% of total segment L, the vcRNA-S accounts for 10% of segment S, and vcRNA-M is even more frequent than the so-called viral strand (52 vs. 48%, respectively).

An important feature of this Direct Nanopore RNA Sequencing approach is its potential to detect the presence of mRNA in purified virions. Indeed, because TSWV mRNAs acquire their cap through a cap-snatching process that adds 12 to 20 nucleotides snatched from host mRNAs (25, 26), it is possible to scrutinize all available 5′ sequences of the viral RNA extracted from purified virions and check for the presence of a stretch of 5′-terminal nonviral (host) nucleotides. Recent detailed studies of Direct Nanopore RNA sequencing reported a loss of the processive control of motor proteins when the end of the RNA molecule is released from the pore, resulting in an arrest of the sequencing process 11 nucleotides from the 5′ extremity (23, 27, 28). We looked at all reads reaching the 5′ region of the TSWV RNAs for all segments and polarities. The number of reads per nucleotide position crashes from about 1,200 to 14 between nucleotide positions 15 and 10 from the 5′ extremity (Fig. 2*B*), indicating an absence of cap-snatching related extension expected in viral mRNAs. Moreover, among the 14 reads that extended beyond the 5′ extremity of the viral RNAs, none could be interpreted as a cap-snatched sequence. The first reason is that all but one of these 5′-extensions were much too long, between 56 and 1,035 bases; the remaining one was only six nucleotides long. The second reason is that, when blasting solely the first 30 nucleotides of these 14 extensions (Fig. 2*C*), we could not find a single significant match which could indicate the presence of a short sequence snatched from a host mRNA (BLASTn searches against Viridiplantae or Solanaceae accessions). Our conclusion is thus that the TSWV particles do not package even minute amounts of viral mRNA.

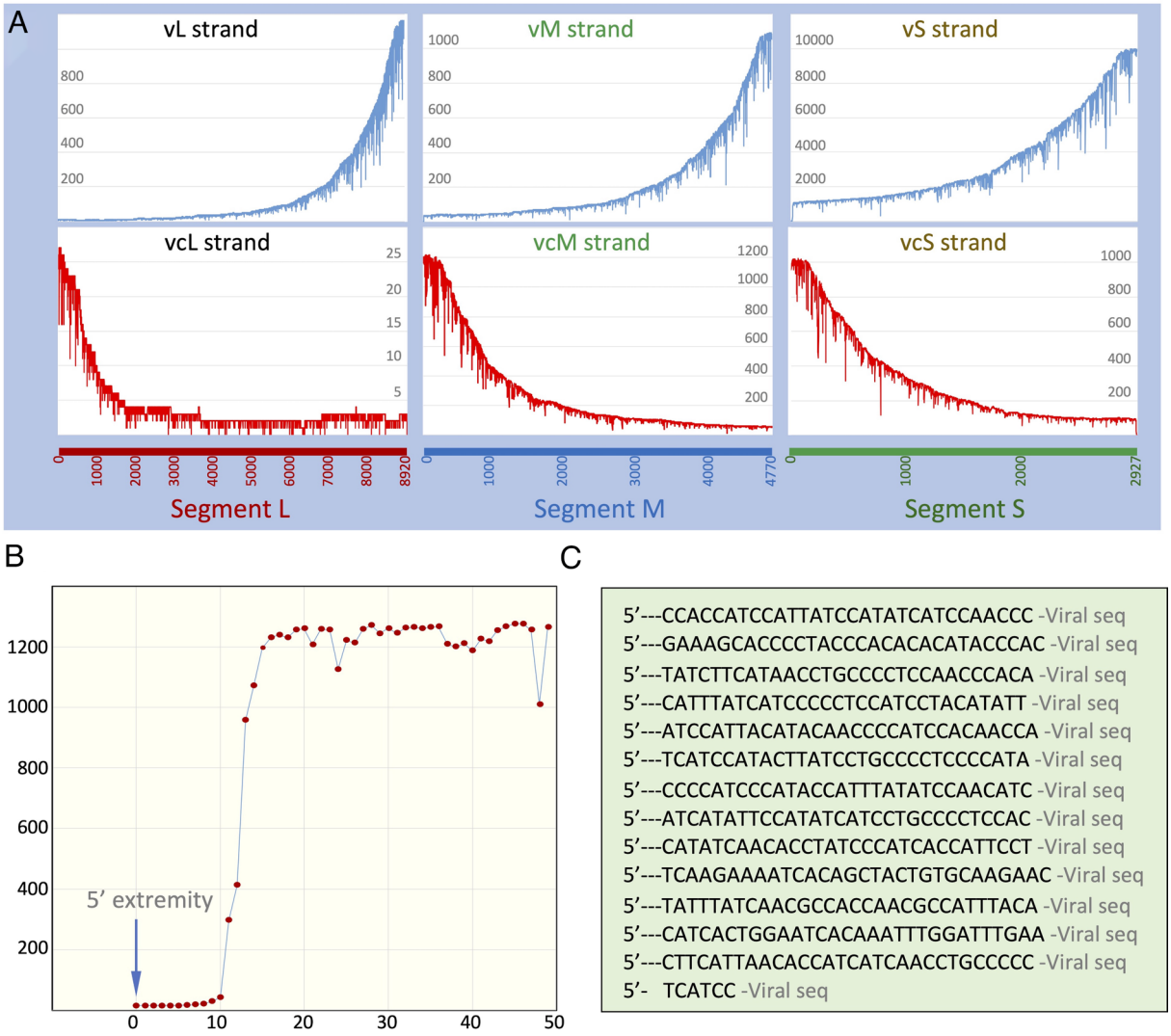

Fig. 2. Direct RNAseq of viral RNAs extracted from purified virus particles. (*A*) Sequencing depth (scale is indicated within each individual panel) per nucleotide position for L, M, and S segments. The three genome segments in the viral orientation are illustrated by a colored thick line under the graphs where nucleotide numbering is indicated. Sequencing reads for the viral (v) and viral complementary (vc) strands are respectively shown in blue (*Top* panels) and red (*Bottom* panels). Row data of the RNAseq are available at https://www.ncbi.nlm.nih.gov/sra/PRJNA1020112. (*B*) Sum of the number of reads at nucleotide positions from 50 to 0 from the 5′ extremity of all six RNA species shown in *A*. The sequencing proceeds from the 3′ toward the 5′ end of the molecule, so from right to left on the graph. The sequencing depth per nucleotide position appears stable when the sequencing progresses from position 50 to position 15 toward the 5′ extremity, but totally crashes between position 15 and position 10, demonstrating an arrest of the sequencing process when approaching the 5′ extremity. (*C*) Among the >1,200 reads reaching the 5′-terminal regions of any of the six viral RNA species (*B*), only 14 extended beyond position 0 (extension length from 6 to 1,035 bases). This panel shows trimmed 30 nucleotide-long sequences extended immediately upstream of the 5′ end of the viral segment in these 14 cases. Note that the bottom sequence had only six nucleotides while all others had more than 30.

Strand-Specific qRT-PCR Confirms the Presence of Viral and Complementary Strands of the Three Segments Each at a Specific Frequency in a Population of TSWV Particles. As further debated in the *Discussion*, the quantitative accuracy of Direct Nanopore RNA sequencing is not established, and thus, we had to confirm our conclusion with an unrelated and accurate quantitative technology. We developed and thoroughly validated a strand-specific qRT-PCR approach (*Materials and Methods*) and first applied it to the viral RNA sample used for Direct Nanopore RNA Sequencing for comparison (Fig. 3*A*). The result that is strikingly consistent across the two techniques is the presence of the viral complementary strands for all three segments, with the lowest proportion for L (~10% of total L), followed by S (~30% of total S) and an astonishing near 60% of total M. Although the general trend is the same, it is noticeable that the frequency estimates of the distinct viral RNA species differ between Direct Nanopore RNA Sequencing and qRT-PCR. This specific technical point will be addressed in the *Discussion*.

The presence of large proportions of viral complementary strands was a surprise. We ascertained that the RNA extracted from virus particles with our protocol does not contain considerable amounts of "free" RNA in solution or RNA externally associated with viral membranes. We repeated the purification of virus particles from another infected plant and treated half of it with RNAse prior to qRT-PCR, in order to eliminate all RNA not protected in virus particles. The estimates of the relative proportions of all six viral RNA species obtained before and after this treatment are quasi-identical (Fig. 3*B*), confirming that the viral complementary strand of all three segments is indeed packaged. The total amount of RNA was however drastically reduced by this treatment (four times less RNA after treatment), suggesting that the RNAse can also degrade packaged RNAs though likely at a slower pace. We repeated this experiment after adding in vitro transcripts of a region

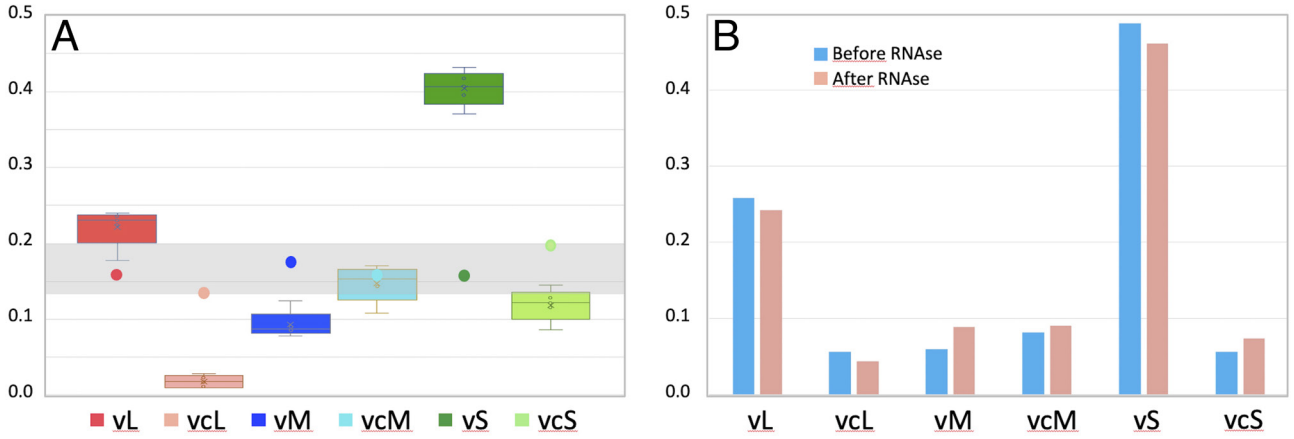

Fig. 3. Relative frequency of each RNA segment and polarity packaged in purified virions. (*A*) The relative proportion of each of the viral RNA segments and polarities was estimated by strand-specific qRT-PCR in a purified TSWV particle preparation (the very same preparation as that sequenced in Fig. 2). The estimate was repeated with four distinct dilutions of the same purified virions preparation: 1-1/10-1/100-1/1000 and the variance engendered by repeated measures and/or dilutions is presented as boxplots. The gray band indicates the range of values within which we estimated the relative frequency of six artificial in vitro transcripts, each corresponding to the qRT-PCR targeted region of a segment-polarity, after attempting to mix them at an equal ratio. The respective estimate for each of the transcripts within this artificial mix is indicated by a colored dot. (*B*) The relative proportion of each of the viral RNA segments and polarities was estimated in another purified TSWV particle preparation, obtained from a different infected host plant, either with (pink) or without (blue) RNAse treatment as indicated in the *Results*.

of the vRNA-M, encompassing the amplified region, to the purified virus suspension. The added amount of soluble RNA should increase the vRNA-M copy number 84 times. This artificially enlarged proportion of vRNA-M totally disappeared after RNAse treatment confirming that the additional free RNA has been completely degraded. In this experimental repeat, the total amount of all packaged RNA species was also decreased to nearly a third, again showing that the RNA packaged into virions can be degraded by prolonged RNAse treatments, but much more slowly than free RNA. Of note is the fact that the degradation of packaged RNA by the RNAse treatment is similarly acting on all RNA species, as their relative proportion remains constant (Fig. 3*B*).

The Viral and Complementary Strands of the Three TSWV Segments Are All Packaged Nonspecifically. When comparing the two preparations of purified virus particles in Fig. 3 *A* and *B*, each from a distinct infected plant, it is noticeable that the relative frequencies of the six viral RNA species (designated hereafter as the genome formula) are alike, though some slight differences are visible. This observation immediately calls for two questions. Is the genome formula reproducible across virus populations from distinct individual host plants? And if yes, does it stem from deterministic selective/specific packaging mechanisms or does it simply reflect the amount of each of the six viral RNA species accumulated in plant tissues during the infection cycle? To answer these questions, we ground one infected leaf from each of the 24 host plants infected in parallel. The resulting 24 crude extracts were then each split into two parts, one for total RNA extraction and the other for virus particle purification followed by RNA extraction. All samples were then submitted to our strand-specific qRT-PCR protocol and the genome formula in total infected plant tissues and in purified virions extracted thereof were compared (Fig. 4).

In total plant extracts, when summing up the number of copies of a given segment for both viral and complementary strands, we obtained an L/M/S ratio of approximately 1/1/3. This overall segment ratio can be compared with most semi-quantitative estimates found in the literature for other bunyaviruses (for example, see refs. 11–13, 17, and 21), where the viral and complementary RNA strands were not distinguished. In contrast, accurately quantifying the two polarities for each segment is more complex, and such a comprehensive genome formula, established in a large set of host individuals infected in parallel, has not been reported before for any species in the order *Bunyavirales*.

In extracts from purified virus, the total number of copies of all 6 viral RNA species was 72 times lower than in leaf extracts. This difference may in part stem from a loss of virions during the purification process, but it also suggests that high amounts of viral RNA may exist in the host plant in a nonpackaged form. The genome formula of viral RNAs packaged in virion populations appears strikingly similar to that of total RNA in infected plant tissues. For one out of the six RNA species (for vM), the relative frequency estimated from total plant extracts and from purified virion preparations is not statistically different. For the other five RNA species (vL, vcL, vcM, vS, and vcS), differences are statistically significant but always of very a small magnitude, still consistent with the genome formula being similar in total plant extracts and in purified virions.

Another way to compare the proportion of the viral RNA species in infected cells and in purified virus particles is to test for a possible correlation between the relative frequency of a given viral RNA species in the 24 plant extracts and in the corresponding 24 populations of virions. Remarkably, a positive and statistically significant correlation was revealed in three out of six cases: vL, vS, and vcS. The linear regression equation and the results of the tests for these three RNAs are vL: Freq_vL(particles) = 0.0958832 + 0.7074039*Freq_vL(plants), R^2 = 0.28, test on slope: t-ratio = 2.91, Prob > |t| = 0.0081; vS: Freq_vS(particles) = 0.2432724 + 0.4215708*Freq_vS(plants), R^2= 0.27, test on slope: t-ratio = 2.84, Prob > |t| = 0.0095; vcS: Freq_vcS(particles) = 0.0194624 + 0.4119993*Freq_vcS(plants), R^2= 0.84, test on slope: t-ratio = 10.68, Prob >|t| < 0.0001).

Together, these results indicate that the viral and complementary strands of each of the three TSWV genome segments are accumulated at specific and reproducible levels during the infection of a given host plant species, and that they are packaged nonspecifically preserving a similar frequency pattern at the level of the viral population.

Discussion

As detailed in the introductory paragraphs, numerous previous reports scattered across multiple virus species in the order *Bunyavirales* have provided evidence or hinted at the possibility

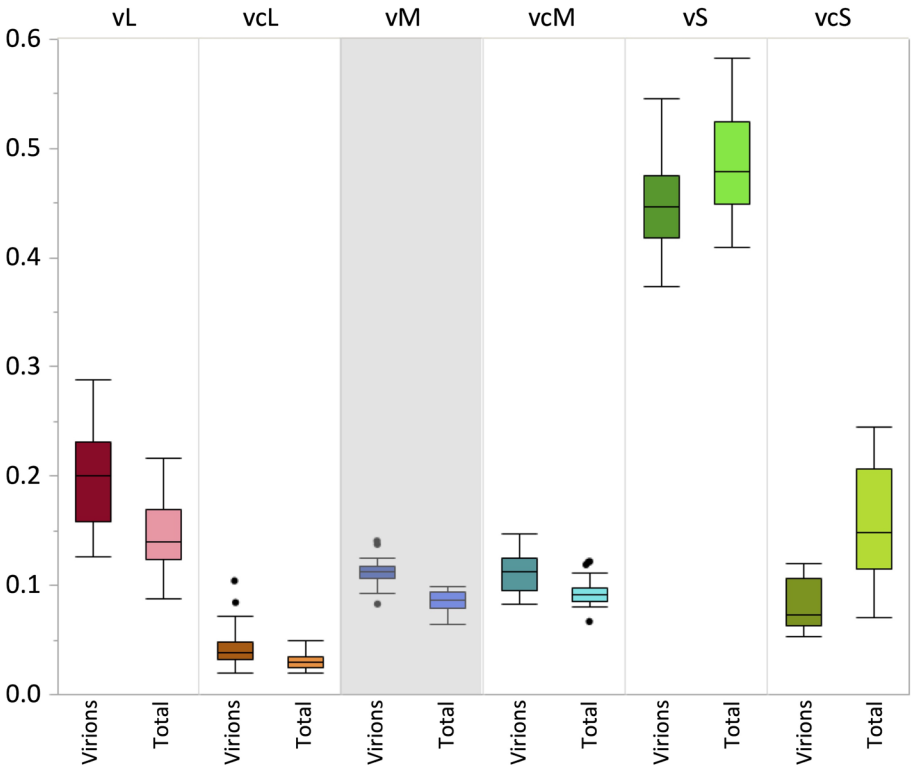

Fig. 4. Comparison of the relative frequency of each RNA segment and polarity in packaged and total viral RNA. The relative proportion of each of the viral RNA segments and polarities was estimated by strand-specific qRT-PCR either in total RNA extracts from infected plant leaves (Total; n = 24) or in virions purified from these leaves (Virions; n = 24). The results are represented as box plots with the horizontal bar indicating the median value of the distribution. The identity of the viral RNA is indicated above the graph. Statistical analysis was performed as indicated in the *Materials and Methods*. The gray-shaded panel indicates the RNA species for which the difference in frequency observed in total RNA extracts and in purified virions is not statistically significant. The segments' frequencies calculated from qRT-PCR on these 48 samples are available in Dataset Table S2.

that virions in this group often deviate from the canonical view by not packaging exactly one copy of each genomic segment and further that viral complementary strands may be packaged. How often and to what extent the real situations deviate from this canonical view, and how this could affect the understanding of major aspects of the biology of bunyaviruses remained largely unclear. Earlier studies consistently revealed an important heterogeneity of the genetic material contained in individual virions. Hence, it is unclear what is to be considered the genome of these viruses and whether it should be defined at the virion level or, more meaningfully, at a larger scale. Using TSWV as a model species, we have confirmed and formally quantified the stunning heterogeneity of virus particles and characterized the RNA species that can be packaged and in what proportions. In addition, we have demonstrated that the genetic heterogeneity at the virion level is structured in a reproducible manner at the population level, extending the concept of genome formula, developed to better describe the biology of multipartite viruses, to the TSWV and perhaps beyond, to the *Bunyavirales* large group of segmented viruses.

The size distribution of viral particles has been earlier estimated for two other bunyaviruses, LACV (9) and UUKV (10). The amplitude of the size variation is comparable in all three bunyaviruses (including TSWV studied here) and higher than that of other segmented viruses which were shown to possess specific packaging mechanisms of their genome segments, such as, for example, influenza virus A (29) and rotaviruses (30). Notably, the size variation estimated here for TSWV is even more important than that of birnaviruses (31) which have been shown to encapsidate their two genomic segments in a nonspecific manner, often packaging more than one copy of each (32). The size distribution appeared unimodal in previous studies on bunyaviruses and, in one case, was qualified as "normal" (10). However, the number of particles used for these estimates was relatively low, respectively 350 and 165, and the corresponding graphs seemed to reveal more particles that were smaller than the modal value. In our experiment, the size distribution of 4,861 TSWV particles follows a near-symmetrical distribution, indicating that the number of smaller particles is similar to larger ones and that both become equally infrequent as the distance to the modal value increases (Fig. 1*B*). Intriguingly our results do not support earlier speculation that virion size variation correlates with the amount of RNA content (9). We observed remarkable variability in the quantity of packaged RNA (volume of electron density within virions), with some particles containing a volume of genetic material four times larger than others, even among particles with the smallest diameters between 70 and 75 nm (Fig. 1*D*). This lack of correlation between particle size and RNA content is consistent with the observation that particles of UUKV can form without encapsidating any genetic material (22, 33). A comparison of the size distribution of empty particles may reveal that diameter and volume of virions are determined by the sole physical properties of the association between membranes and glycoproteins. It is also possible that the packaging of the viral genetic material depends on the amount of RNA that is locally and temporarily available. In any case, this observation further extends the heterogeneity of packaged RNA, as this heterogeneity is also large among particles of the same size class. In some of the observed viral particles, the tomographic analysis reveals poorly resolved distinct inner density volumes within a single virion, each potentially corresponding to

a distinct segment. We observed from one to four such distinct volumes per virion, consistent with the recent demonstration that particles of RVFV can package a very variable number of segments (15, 17). In contrast, we did not observe any particle with a complete absence of inner density, suggesting that empty particles are very rare in TSWV and in our experimental setup while they appear very frequent in RVFV (15). One important caution is that, due to low resolution of our tomographic analysis, the assignment of each distinct inner density volume to one individual segment may not be totally reliable. Heterogeneous local compactions (34, 35) and the extreme flexibility (35) of a single segment may sometimes appear as more than one distinct volume upon tomography 3D reconstruction, and two closely packed/entangled segments may appear as a single larger volume. Higher-resolution cryo-EM tomography will be required to solve the question of the spatial arrangement of the segments and to reveal the range of the identity and number of segments potentially co-packaged in individual virions.

The packaging of viral complementary sense RNA has been reported for segment S of UUKV (18), for segment M of LACV (36), for segments M and S of TSWV (13), and more recently for segments S, M, and L of RVFV '(15, 19). In these papers, the possible biological impacts of packaging the two polarities of a segment have been discussed, the most obvious one being a putative benefit of early expression of some of the genes due to immediate availability of both strands. This would concern primarily ambisense segments, where the ratio of vRNA vs. vcRNA may make one or the other of the two genes encoded in opposite orientation expressed early or late (18, 19). It seems less evident, however, for negative-sense RNA segments for which the vcRNA strand (which is not capped) cannot be translated before de novo transcription from the vRNA where cap-snatching occurs (thus they cannot be translated earlier than vRNA). Consistent with this argument, the vcRNA of the negative-sense segment L of TSWV could not be detected within virions in earlier studies (13). In contrast, the vcRNA of the negative-sense segment M of LACV was detected (36), leading the authors to conclude on a possible artifactual misincorporation. Going beyond detection, some of these studies provided "semi-quantitative" estimates. For example, Kormelink and colleagues clearly mentioned that the M segment was the one with the highest amount of packaged vcRNA for TSWV, though still largely lower than the vRNA. Here, with two distinct technologies, Direct Nanopore RNA Sequencing and strand-specific qRT-PCR, we establish that TSWV packages both polarities of its three segments L, M, and S. The quantification of all 6 RNA species by these two techniques reveals very consistent trends, with the abundance of packaged vcRNA being M > S > L. However, the exact relative copy number varies considerably depending on the technique and this is further discussed in the next paragraph. Of note here is the general consensus that mRNAs of bunyaviruses are not significantly packaged into virions because they lack the sequence driving their interaction with (and coating by) the nucleoprotein (13, 15, 18, 19, 37). However, with the techniques used earlier for mRNA detection within purified virus preparations, minute amounts of subgenomic mRNA might have been overlooked, and hence, this was still considered a possibility (15). Here, we used the direct RNAseq approach to examine the 5′ extremity of the packaged viral RNAs, in search for snatched host sequences. Out of >1,200 RNA 5′-extremities analyzed, not even a single mRNA molecule could be identified, confirming that TSWV does not package mRNAs, at least not at a level that could be considered biologically significant.

Because direct RNAseq and strand-specific qRT-PCR did not reveal the same proportion of vRNA vs. vcRNA, particularly for segments L and S, we set up an experiment intended to control the accuracy of the strand-specific qRT-PCR (*Materials and Methods* and Fig. 3*A*). Conceptually, it is very simple and consists of producing a solution containing a mix of the 6 RNA species from in vitro transcripts in a known ratio, here 1/1/1/1/1/1, and submit it to the qRT-PCR. The resulting estimates were close to the expected relative frequency of 16.6% for each of the six RNAs, the largest deviation being an observed frequency of 20% (Fig. 3*A*, gray horizontal band). We believe these deviations are small insofar as they may arise because the ratios in the initial control mix were not exactly equal. Indeed, quantifying transcripts in solution by spectroscopic methods is poorly accurate due to variable sequence-related secondary structures engendering highly variable proportions of single- or double-stranded regions. For this reason, and because the quantitative power of the Direct Nanopore RNA Sequencing is not established (24, 27, 28), in this and future work, we consider the strand-specific qRT-PCR approach as the more accurate and reliable.

In any case, as revealed with both RNAseq and qRT-PCR, the vcRNA-M is extremely frequent, even more frequent than the vRNA-M. According to qRT-PCR estimates, vcRNA-S and vcRNA-L respectively represent 30% and 8% of the total corresponding segment RNAs. With such high amounts of packaged vcRNAs, our results again question what should be considered the viral genome, v- or vc-strand. More interestingly, they also render unlikely the possibility that packaged vcRNAs are biologically irrelevant. Beyond previous speculations, on a regulatory role for gene expression kinetics at the early stages of infection(13, 18, 19), numerous additional questions are raised: Can v and vcRNA of a same segment be co-packaged in the same virion or are they necessarily separated in distinct particles and only together at the population level? Does a virion with the vRNA of a given segment and another virion with the vcRNA of the same segment have similar infectivity? Does this also depend on the polarity of the other segments in the same virion? Do the putative distinct properties of individual virions make any sense at the population level through complementation and/or cooperation? Our findings provide a foundation opening important issues for future research on the order *Bunyavirales*, beyond TSWV and the family *Tospoviridae*.

Among the above nonexhaustive list of possible questions, those that appear particularly novel are at the population level. If v- vs. vcRNA segment ratios have a functional role, this can only be conceived at the population level. It is indisputable that the RNA content of individual virions is highly heterogeneous in RVFV (15, 17) and as indicated here in TSWV. We therefore made use of the TSWV system to investigate the genetic composition at the population level. First, in all plants of one species, so in one given environment, TSWV populations produce a very similar frequency pattern for the six viral RNA species. This situation is remarkably reminiscent of the genome formula described for multipartite viruses (38–40), where distinct parts of the genetic information are packaged separately in distinct virus particles, but very reproducibly accumulate at the population level. While a phenomenon such as the genome formula with unequal ratios could be anticipated for other bunyaviruses within infected cells with unpackaged genomic segments (14, 41), the situation was less predictable in purified virions as it depends on whether the packaging process constrains these ratios. Some earlier studies reported comparable segment frequency patterns in infected tissues and in purified virions(13, 15, 17), whereas others noted a variability of this pattern depending on the virus particle preparation (14, 18). To resolve this issue in TSWV, we used a large set of infected plant replicates to compare the genome formula in infected leaves and in virions

from these leaves. Beyond revealing very similar formulas, more convincing was the demonstration that the small variations of a viral RNA frequency observed across the leaf extracts correlate with those observed across the corresponding virus preparations. Despite an unavoidable experimental "noise" induced by purification steps, RT and qPCR, such correlations could be detected for three out the six analyzed RNA species (vL, vS, and vcS). This experimental noise and the low variations of the less frequent segments/polarities may explain that correlation was not detected in the three other cases. These unique observations empirically confirm that the viral RNA species accumulating during the infection cycle within a host are packaged according to their frequency, thus with no apparent specific mechanisms that would bias the ratios.

In the same view as that currently developing for multipartite viruses (40, 42), one could imagine that bunyaviruses can have emerging properties at the population level (all virions being different) that would be driven by the genome formula. Whether the genome formula controls gene expression (14, 39), whether it is adjustable depending on the environment (15, 43) (including within insect thrips vectors), whether virions with distinct and incomplete genetic information can be transmitted cell-to-cell and host-to-host separately (44–46), and, most of all, whether they can proficiently complement in natural situations are all new research horizons for the biology of bunyaviruses.

Materials and Methods

Plants, Growth Conditions, Inoculation, and Sampling. All plants were seeded and maintained in a growth chamber with a 16/8-h day/night photoperiod, a constant temperature of 20 °C, and 70% hygrometry. The TSWV isolate used in this study is the TSWV MR-01 (47), maintained as a −80 °C frozen stock of *Datura stramonium* (L.) leaves collected from plants initially infected through transmission by the natural thrips vector *Frankliniella occidentalis* (Pergande). *Nicotiana rustica* (L.) plantlets at the sixth leaf stage were mechanically inoculated on their fourth leaf, by rubbing a virus suspension prepared from the frozen stock with 1 g of infected leaves ground in 3 mL of 0.01 M phosphate buffer (pH 7.5) with the addition of Carborundum or Celite abrasive powder. Three weeks post-inoculation, 1 g of the sixth leaf of each systemically infected plant was collected for further RNA or virus particle purification.

Total RNA Extraction and Virus Particle Mini-Prep Protocol. One gram of infected leaf tissue was homogenized for 20 s with four ceramic beads in 3 mL EB (Extraction Buffer: 0.1 M sodium phosphate, pH 7, containing 0.01 M Na_2SO_3) in a 15-mL Falcon tube, using the FastPrep MP grinding machine. Of these crude extracts, 200 µL could be used for total RNA extraction using the Monarch Total RNA Miniprep kit (NEB #T2010, final elution in 50 µL RNAse-free water and storage at −80 °C) according to manufacturer instructions and the rest for further virus purification as described hereafter. Crude extracts were filtered through a Luer Terumo syringe stuffed with Miracloth and centrifuged at 4 °C and 10,000 g for 15 min. The supernatant was discarded, and the pellet was rinsed with RB buffer (Rinse Buffer: 0.01 M sodium phosphate buffer, 0.01 M Na2SO3, pH 7) and rapidly resuspended in 2 mL RB using a tissue grinder. After 15 min of 8,000 g clarification at 4 °C, the supernatant was collected and passed through a 5 mL Terumo Syringe containing a ClearLine Syringe 30 mm AC 0.2 µm filter. Two to 2.5 mL of the filtrate were then overlaid on a 10 to 40% sucrose gradient, prepared in an Ultra Clear Tube for the SW41 rotor and centrifuged at 70,000 g for 1 h at 4 °C in a Beckman SW41 rotor. The opalescent band appearing in the gradient was collected, diluted with RB 1/12 in a 13-mL polycarbonate tube, and pelleted for 1 h at 70,000 g and 4 °C. The pelleted virions were finally resuspended in 150 µL sterile double-distilled water. When larger amounts of purified virions were necessary, several samples could be pooled together in the same 15-mL falcon tube after the Miracloth first filtration step. In some instances, viral RNA was extracted from purified virions exactly as from plant crude extracts.

Cryo-EM and Estimation of the Diameter of Virus Particles. Three microliters of freshly purified TSWV particles were overlayed onto a glow-discharged Quantifoil R 2/2 grid covered with a 2- to 3-nm ultra-thin carbon layer (Quantifoil Micro tools GmbH), blotted for 1 s to eliminate the extra-volume and then flash frozen in liquid ethane using a CP3 cryoplunge (Gatan Inc.). Before freezing, the humidity rate was stabilized at about 95%. Cryo-EM was carried out on a JEOL 2200FS FEG microscope operating at 200 kV under low-dose conditions (total dose of 20 electrons/Å^2), in the zero-energy-loss mode with a slit width of 20 eV. Images were taken at a nominal magnification of 50,000×, corresponding to a calibrated magnification of 45,591× with defocus ranging from 1.5 to 3.0 µm, using a 4 k × 4 k slow scan CCD camera (Gatan, Inc.). The diameter estimation of TSWV particles was performed using ImageJ (48).

Electron Tomography and Segmentation. First, 300 µL of purified virus particles suspension was fixed by addition of glutaraldehyde (5% final concentration) and incubated for 45 min at 4 °C. Fixed virions were then diluted in 8 mL of RB and ultracentrifuged at 31,000 g for 1 h at 4 °C to eliminate the fixing agent. The pellet was resuspended in 50 µL RB and added with a small volume of Chinese ink to dark stain the sample. Then, 100 µL of 3% low melting agarose (35 °C) was added and homogenized before cooling overnight at 4 °C. The jellified dark block was then extracted from the tube and post-fixed for 1 h at 4 °C with 1% osmium tetroxide, rinsed three times in 0.1 M cacodylate buffer, and dehydrated in a series of acetone solutions as follows: two 10-min bathes of each of 50, 70, 90, and 100% acetone at 4 °C. The dehydrated agarose block was imbedded at room temperature in 25% TAAB resin in acetone for 3 h, in 50% TAAB resin in acetone overnight, in pure resin for at least 3 h, and transferred in silicon molds filled with resin. The resin block was finally polymerized one night at 56 °C. Thin sections of 200-nm thickness were prepared using an ultramicrotome (LKB ultratome NOVA) and contrasted for 20 min in 2% uranyl acetate followed by 3 min in 2% lead citrate.

Series of tilted images from semi-thin sections of embedded TSWV particles were collected on a JEOL 1400 Flash electron microscope, operating at 120 kV at a magnification of 15,000×, using a Oneview camera (Gatan, Inc.) with defocus values ranging from −3 µm to −5 µm. The acquisition was performed semi-automatically using SerialEM (49). Tilt series consisting of about 60 images were collected by tilting the specimen between −60° and 60°, imaging at 2° increments, with a total dose of about 700 electrons/Å^2. Image alignment and three-dimensional reconstructions were performed using Etomo from IMOD package (50). Segmentations of particles were done using Amira software (Thermo Fisher Scientific).

Direct Nanopore RNA Sequencing. Total RNA was isolated from 600 µL of purified virions suspension using the Monarch Total RNA Miniprep kit (NEB #T2010) and quantified using the Qubit 3.0 fluorometer (Life Technologies, Carlsbad, CA). RNAs were poly(A) tailed using the *Escherichia coli* Poly(A) Polymerase NEB M0276 kit (New England BioLabs) and further purified using paramagnetic beads supplied by the RNAClean XP kit (Beckman Coulter). The Nanopore sequencing library was constructed using the Direct RNA Sequencing Kit (SQK-RNA002), following the manufacturer's instructions. Direct sequencing of the poly(A) tailed RNAs was then performed on one R9.4.1 Flongle flow cell (FLO-FLG001) using MinKNOW software 22.03.5.

Accurate base calling was performed using Guppy (v6.1.2; Oxford Nanopore Technologies, available online: https://nanoporetech.com/) in super accuracy mode (sup) and consensus filtered for a minimum Q-score quality of 7. Adapter removal was then achieved using Porechop v0.2.4 (available online: https://github.com/rrwick/Porechop). Quality of the reads was investigated using NanoPlot v1.40.0 (51). Cleaned reads were further mapped in the two orientations with a High/Medium Sensitivity on the three segments of TSWV isolate MR-01 (segment S, accession number MG593199.1; segment M, accession number MG593198.1; segment L, accession number MG593197.1) using Geneious 5.5.9 (Biomatters Ltd.). Coverage of each base of each segment was then recovered. Finally, mapped reads were filtered into two groups, one large group of reads with no additional bases at the 5′-end of the viral genomic RNA, and a very small group of only 14 reads having an extension at the 5′-end of the viral genomic RNA.

As a quantitative approach, we simply counted the number of reads that were initiated at the 3′ end of each of the distinct viral RNAs. We considered that this represents the number of copies of a given RNA species entering a sequencing pore, which may reflect its frequency in the sequencing library. To the best of our knowledge, how distinct RNA sequences could bias this quantitative estimate due to secondary structures or to other reasons is thus far undetermined.

Strand-Specific RT and qPCR. From the extracted viral or total RNA, we aimed at quantifying specifically the viral strand (vRNA) and the viral complementary strand (vcRNA) of each of the three genomic segments S, M, and L, avoiding the co-quantification of viral mRNAs whenever possible. Classic qRT-PCR primer design revealed an auto-priming problem. We adapted an approach developed earlier to solve a similar issue with the rift valley fever virus (52). This technique involves use of a unique 20 nucleotide-long Tag-sequence fused at the 5′ extremity of the RT primer. Because the Tag-sequence is later used as one of the primer pair designed for qPCR, all cDNA generated by "auto-priming" (i.e., cDNA nonspecifically primed by secondary structures or by co-purifying small RNAs produced in the infected host) and thus lacking this Tag-sequence will not be amplified. A common Tag-sequence was used for the six specific RT primers (Dataset Table S1-A), as well as for all forward primers for subsequent qPCR, the specificity at this latter step being therefore determined by the reverse qPCR primers (Dataset Table S1-A). It is important to note that the distinct primer sets for qRT-PCR target plus or minus sequence strands either in the 5′ or 3′ halves of the ambisense M and S segments. For a given polarity, the chosen region was that where the subgenomic messenger RNAs do not overlap, avoiding the co-amplification of the M and S segments together with their mRNA. Unfortunately, for segment L, the mRNA is full length and so our approach cannot distinguish the amplification of the vcRNA-L from that of the mRNA, in total RNA extracts from infected plants.

Before RT, the purified viral or total RNA was diluted 1/100 with RNAse-free water. Four microliters of this dilution was used as a template, added with the RT Tagged-primers (10 μM final concentration), and the mixture was heated at 70 °C for 5 min to eliminate secondary structures that could hinder the RT efficacy. The mixture was then chilled on ice for 5 min, complemented with avian myeloblastosis virus (AMV) reverse transcriptase (Promega), and processed according to the manufacturer's specifications. After RT, qPCR reactions (40 cycles of 95 °C for 10 s, 60 °C for 10 s, and 72 °C for 10 s) were carried out using the LightCycler FastStart DNA Master Plus SYBR green I kit (Roche) in a LightCycler 480 thermocycler (Roche), following the manufacturer's instructions. Two microliters of the RT products diluted 1/10 was used as qPCR template, and the primers were adjusted to a final concentration of 0.4 μM. The fluorescence data were analyzed with the LinReg qPCR program (53). Relative frequencies were then calculated in each sample by dividing the estimated absolute fluorescence value (N0) of a given segment by the sum of the N0 of all six segments (three cDNA viral sense and three cDNA viral complementary sense).

RT is obviously a key step in the quantification of the different segments and polarities, because in contrast to the qPCR, there is no evaluation and correction for possible different efficacies on different RNA sequence targets. We first verified that multiplexing the 6 RT reactions (vRNA and vcRNA for segment L, M, and S) in a single tube did not bias the results of subsequent qPCR on the corresponding cDNAs, as compared to the 6 RTs being carried out separately (Dataset Table S1-B). This possible bias being relaxed, we then experimentally controlled the accuracy of the quantification of the relative copy number of the 6 distinct viral RNA species. We produced in vitro transcripts encompassing the six amplified sequences, quantified each of these transcripts with a NanoDrop 2000 (RNA mode), mixed them at an equimolar ratio with a total RNA final concentration of 2.92 ng/mL, and estimated their relative copy number with our strand-specific qRT-PCR protocol (see *Results*, Fig. 3*A* and *Discussion*).

Plasmids Construction and In Vitro Transcription. cDNAs covering the whole TSWV MR-01 genome sequence were synthesized from TSWV-infected *Nicotiana rustica* (L.) plant leaves with random primers using iScript RT Supermix kit (Biorad). From these cDNAs, PCR primers (Dataset Table S1-A) were designed to amplify about 450 nucleotides from two distinct regions of genomic RNA L (nucleotide position 599 to 1003 and 7918 to 8322), RNA M (291 to 718 and 2844 to 3322) and RNA S (nt 261–689 and 2106 to 2522), using the 2× PCR master mix (Promega), PCR Reactions were done in a thermocycler (Eppendorf) first set at 95 °C 2 min, followed by 30 cycles of 95 °C 30 s, 55 °C 30 s, 72 °C 30 s, and finally 72 °C 15 min. PCR products were cleaned using Wizard SV Gel and PCR clean-up system (Promega) and cloned into pGEM-T Easy vector syst (Promega). All resulting plasmids had one of the TSWV short sequences indicated above flanked on one side by SP6 promoter and on the other by T7 promoter. SP6 or T7 could later be used for in vitro transcription depending on the orientation of the cloned TSWV sequence and the desired polarity of the transcript. The orientation and integrity of each of the cloned TSWV sequences was verified by sequencing.

Three to five micrograms of each of these plasmids were linearized by digestion with Sal I or Nco I (New England Biolabs), followed by enzyme inactivation at 80 °C for 20 min. Transcriptions to generate the desired plus-strand or minus-strand RNAs were done using SP6 (Nco I digests) or T7 (Sal I digests) using the Maxiscript kit (Invitrogen), according to the manufacturer recommendation. The template plasmids were then eliminated by DNAse1 (RNAse-free) treatment (Invitrogen), and the RNA finally precipitated with 0.5 M Ammonium Acetate and 70% ethanol, rinsed, and stored in water at −80 °C.

Statistical Analysis. The histogram of the diameter distribution of virus particles was fitted to a normal distribution and the significance of the fit was assessed by the Kolmogorov–Smirnov test.

To test whether the frequency of the six viral RNA species (segment and polarity) differed between total plant extracts and purified virus particles, we performed an ANOVA using the model logit(frequency_RNA species) = treatment * RNAspecies + 1|replicate plant, where treatment corresponds to total plant extracts vs. purified virus particles. A difference in the frequencies of RNA species across treatment modalities is thus indicated by a statistically significant treatment by RNA species interaction. For each RNA species, the statistical significance of the difference in frequency across treatment modalities was assessed by Tukey's HSD test. The identity of the replicate plant is introduced in the model as a random effect to account for the fact that each replicate plant yielded both total plant extracts and purified virus particles which are thus statistically paired.

The correlation of each RNA species frequency across treatment modalities was tested using linear regressions on the frequencies of the RNA species (linear regressions on the logits of the frequencies yielded very similar results and are not presented).

These three analyses were performed using JMP 13.2.1 software (SAS Institute 2016).

Data, Materials, and Software Availability. All microscopic and PCR data produced are visible in the figures and *SI Appendix*. In particular, Dataset Table S2 contains all segments' relative frequency calculated from qRT-PCR to build Fig. 4. Nanopore RNA sequencing data are available at https://www.ncbi.nlm.nih.gov/sra/PRJNA1020112. All other data are included in the manuscript and/or supporting information.

ACKNOWLEDGMENTS. We are deeply thankful for the contribution of our colleague T.L.G. and for his timeless imprint on this work. We are grateful to MUSE Univ Montpellier for funding this work (project BLANC-MUSE2020-Multivir). M.Y., E.V., P.G., M.-S.V., and S.B. acknowledge support from INRAE department SPE; Y. Michalakis from CNRS and IRD; P.B., J.L.K.H., A.A., and J.G. from INSERM; E.F., D.F., and P.R. from CIRAD. D.E.U. acknowledges support from the Fulbright Scholar Program and sabbatical leave from University of California Davis. T.L.G. acknowledges funding for this work was provided in part by the USDA-ARS Floriculture and Nursery Research Initiative project# 58-6034-5-029. We thank Jean-Marc Leininger and Norma Ordaz for technical support in providing virus isolate.

Author affiliations: [a]PHIM, Univ Montpellier, INRAE, CIRAD, IRD, Institut Agro, Montpellier 34398, France; [b]Department of Entomology, University of Wisconsin, Wisconsin 53706, Madison; [c]Department of Entomology and Nematology, University of California, California 95616, Davis; [d]Pathologie végétale, INRAE, Avignon 84143, France; [e]CBS, Univ Montpellier, CNRS, INSERM, Montpellier 34090, France; and [f]MIVEGEC, Univ Montpellier, CNRS, IRD, Montpellier 34394, France

Author contributions: M.Y., T.L.G., D.E.U., P.R., P.B., Y.M., and S.B. designed research; M.Y., T.L.G., D.E.U., R.D., M.H.P., S.B.-M., E.V., P.G., A.A., J.L.K.H., J.G., M.-S.V., E.F., and P.R. performed research; M.Y., T.L.G., D.E.U., R.D., M.H.P., D.F., P.R., P.B., Y.M., and S.B. analyzed data; R.D. and M.H.P. edited the paper; Y.M. and S.B. secured funds for the project; and T.L.G., D.E.U., Y.M., and S.B. wrote the paper.

1. E. J. Lefkowitz *et al.*, Virus taxonomy: The database of the International Committee on Taxonomy of Viruses (ICTV). *Nucleic Acids Res.* **46**, D708–D717 (2018).
2. J. H. Kuhn *et al.*, 2022 taxonomic update of phylum Negarnaviricota (Riboviria: Orthornavirae), including the large orders Bunyavirales and Mononegavirales. *Arch. Virol.* **167**, 2857–2906 (2022).
3. N. S. Akopyants, L.-F. Lye, D. E. Dobson, J. Lukeš, S. M. Beverley, A novel bunyavirus-like virus of trypanosomatid protist parasites. *Genome Announc.* **4**, e00715–16 (2016).
4. H. Boshra, An overview of the infectious cycle of bunyaviruses. *Viruses* **14**, 2139 (2022).

5. R. Kormelink, J. Verchot, X. Tao, C. Desbiez, The bunyavirales: The plant-infecting counterparts. *Viruses* **13**, 842 (2021).
6. R. M. Elliott, Orthobunyaviruses: Recent genetic and structural insights. *Nat. Rev. Microbiol.* **12**, 673–685 (2014).
7. Viralzone Tospoviridae. https://viralzone.expasy.org/9764.
8. P. J. Wichgers Schreur, R. Kormelink, J. Kortekaas, Genome packaging of the Bunyavirales. *Curr. Opin. Virol.* **33**, 151–155 (2018).
9. Y. Talmon *et al.*, Electron microscopy of vitrified-hydrated La Crosse virus. *J. Virol.* **61**, 2319–2321 (1987).
10. A. K. Overby, R. F. Pettersson, K. Grünewald, J. T. Huiskonen, Insights into bunyavirus architecture from electron cryotomography of Uukuniemi virus. *Proc. Natl. Acad. Sci. U.S.A.* **105**, 2375–2379 (2008).
11. R. F. Pettersson, M. J. Hewlett, D. Baltimore, J. M. Coffin, The genome of Uukuniemi virus consists of three unique RNA segments. *Cell* **11**, 51–63 (1977).
12. R. Pettersson, L. Kääriäinen, The ribonucleic acids of Uukuniemi virus, a noncubical tick-borne arbovirus. *Virology* **56**, 608–619 (1973).
13. R. Kormelink, P. de Haan, D. Peters, R. Goldbach, Viral RNA synthesis in tomato spotted wilt virus-infected Nicotiana rustica plants. *J. Gen. Virol.* **73**, 687–693 (1992).
14. N. Gauliard, A. Billecocq, R. Flick, M. Bouloy, Rift Valley fever virus noncoding regions of L, M and S segments regulate RNA synthesis. *Virology* **351**, 170–179 (2006).
15. E. Bermúdez-Méndez, E. A. Katrukha, C. M. Spruit, J. Kortekaas, P. J. Wichgers Schreur, Visualizing the ribonucleoprotein content of single bunyavirus virions reveals more efficient genome packaging in the arthropod host. *Commun. Biol.* **4**, 345 (2021).
16. S. Murakami, K. Terasaki, K. Narayanan, S. Makino, Roles of the coding and noncoding regions of rift valley fever virus RNA genome segments in viral RNA packaging. *J. Virol.* **86**, 4034–4039 (2012).
17. P. J. Wichgers Schreur, J. Kortekaas, Single-molecule FISH reveals non-selective packaging of rift valley fever virus genome segments. *PLoS Pathog.* **12**, e1005800 (2016).
18. J. F. Simons, U. Hellman, R. F. Pettersson, Uukuniemi virus S RNA segment: Ambisense coding strategy, packaging of complementary strands into virions, and homology to members of the genus Phlebovirus. *J. Virol.* **64**, 247–255 (1990).
19. T. Ikegami, S. Won, C. J. Peters, S. Makino, Rift valley fever virus NSs mRNA is transcribed from an incoming anti-viral-sense S RNA segment. *J. Virol.* **79**, 12106–12111 (2005).
20. P. J. Wichgers Schreur, N. Oreshkova, R. J. M. Moormann, J. Kortekaas, Creation of Rift Valley fever viruses with four-segmented genomes reveals flexibility in bunyavirus genome packaging. *J. Virol.* **88**, 10883–10893 (2014).
21. K. Flick *et al.*, Functional analysis of the noncoding regions of the Uukuniemi virus (Bunyaviridae) RNA segments. *J. Virol.* **78**, 11726–11738 (2004).
22. A. K. Overby, V. Popov, E. P. A. Neve, R. F. Pettersson, Generation and analysis of infectious virus-like particles of uukuniemi virus (bunyaviridae): A useful system for studying bunyaviral packaging and budding. *J. Virol.* **80**, 10428–10435 (2006).
23. R. E. Workman *et al.*, Nanopore native RNA sequencing of a human poly(A) transcriptome. *Nat. Methods* **16**, 1297–1305 (2019).
24. T. Wongsurawat *et al.*, Rapid sequencing of multiple RNA viruses in their native form. *Front Microbiol.* **10**, 260 (2019).
25. R. Kormelink, F. van Poelwijk, D. Peters, R. Goldbach, Non-viral heterogeneous sequences at the 5′ ends of tomato spotted wilt virus mRNAs. *J. Gen. Virol.* **73**, 2125–2128 (1992).
26. S. Olschewski, S. Cusack, M. Rosenthal, The cap-snatching mechanism of bunyaviruses. *Trends Microbiol.* **28**, 293–303 (2020).
27. M. T. Parker *et al.*, Nanopore direct RNA sequencing maps the complexity of Arabidopsis mRNA processing and m6A modification. *Elife* **9**, e49658 (2020).
28. L. Mulroney *et al.*, Identification of high-confidence human poly(A) RNA isoform scaffolds using nanopore sequencing. *RNA* **28**, 162–176 (2022).
29. F. P. Booy, R. W. Ruigrok, E. F. van Bruggen, Electron microscopy of influenza virus. A comparison of negatively stained and ice-embedded particles. *J. Mol. Biol.* **184**, 667–676 (1985).
30. D. Asensio-Cob, J. M. Rodríguez, D. Luque, Rotavirus particle disassembly and assembly in vivo and in vitro. *Viruses* **15**, 1750 (2023).
31. J. Pous *et al.*, Structure of birnavirus-like particles determined by combined electron cryomicroscopy and X-ray crystallography. *J. Gen. Virol.* **86**, 2339–2346 (2005).
32. D. Luque *et al.*, Infectious bursal disease virus is an icosahedral polyploid dsRNA virus. *Proc. Natl. Acad. Sci. U.S.A.* **106**, 2148–2152 (2009).
33. A. K. Overby, R. F. Pettersson, E. P. A. Neve, The glycoprotein cytoplasmic tail of Uukuniemi virus (Bunyaviridae) interacts with ribonucleoproteins and is critical for genome packaging. *J. Virol.* **81**, 3198–3205 (2007).
34. K. Komoda, M. Narita, K. Yamashita, I. Tanaka, M. Yao, Asymmetric trimeric ring structure of the nucleocapsid protein of tospovirus. *J. Virol.* **91**, 1–13 (2017), 10.1128/jvi.01002-17.
35. F. R. Hopkins *et al.*, The native orthobunyavirus ribonucleoprotein possesses a helical architecture. *mBio* **13**, e01405-22 (2022).
36. R. Raju, D. Kolakofsky, The ends of La Crosse virus genome and antigenome RNAs within nucleocapsids are base paired. *J. Virol.* **63**, 122–128 (1989).
37. M. Snippe, R. Goldbach, R. Kormelink, Tomato spotted wilt virus particle assembly and the prospects of fluorescence microscopy to study protein-protein interactions involved. *Adv. Virus Res.* **65**, 63–120 (2005).
38. A. Sicard *et al.*, Gene copy number is differentially regulated in a multipartite virus. *Nat. Commun.* **4**, 2248 (2013).
39. Y. Michalakis, S. Blanc, Editorial overview: Multicomponent viral systems. *Curr. Opin. Virol.* **33**, vi–ix (2018).
40. Y. Michalakis, S. Blanc, The curious strategy of multipartite viruses. *Annu. Rev. Virol.* **7**, 203–218 (2020).
41. C. Rossier, R. Raju, D. Kolakofsky, LaCrosse virus gene expression in mammalian and mosquito cells. *Virology* **165**, 539–548 (1988).
42. A. Sicard, Y. Michalakis, S. Gutiérrez, S. Blanc, The strange lifestyle of multipartite viruses. *PLoS Pathog.* **12**, e1005819 (2016).
43. R. Gallet *et al.*, Gene copy number variations at the within-host population level modulate gene expression in a multipartite virus. *Virus Evol.* **8**, veac058 (2022).
44. A. Sicard *et al.*, A multicellular way of life for a multipartite virus. *Elife* **8**, e43599 (2019).
45. E. Bermúdez-Méndez *et al.*, Incomplete bunyavirus particles can cooperatively support virus infection and spread. *PLOS Biol.* **20**, e3001870 (2022).
46. J. Di Mattia *et al.*, Nonconcomitant host-to-host transmission of multipartite virus genome segments may lead to complete genome reconstitution. *Proc. Natl. Acad. Sci. U.S.A.* **119**, e2201453119 (2022).
47. N. A. Ordaz *et al.*, The Sw-5b NLR immune receptor induces earlier transcriptional changes in response to thrips and mechanical modes of inoculation of Tomato spotted wilt orthotospovirus. *Mol. Plant Microbe Interact.* (2023), 10.1094/MPMI-03-23-0032-R.
48. C. A. Schneider, W. S. Rasband, K. W. Eliceiri, NIH Image to ImageJ: 25 years of image analysis. *Nat. Methods* **9**, 671–675 (2012).
49. D. N. Mastronarde, Automated electron microscope tomography using robust prediction of specimen movements. *J. Struct. Biol.* **152**, 36–51 (2005).
50. J. R. Kremer, D. N. Mastronarde, J. R. McIntosh, Computer visualization of three-dimensional image data using IMOD. *J. Struct. Biol.* **116**, 71–76 (1996).
51. W. De Coster, S. D'Hert, D. T. Schultz, M. Cruts, C. Van Broeckhoven, NanoPack: Visualizing and processing long-read sequencing data. *Bioinformatics* **34**, 2666–2669 (2018).
52. B. Tercero, K. Terasaki, K. Nakagawa, K. Narayanan, S. Makino, A strand-specific real-time quantitative RT-PCR assay for distinguishing the genomic and antigenomic RNAs of Rift Valley fever phlebovirus. *J. Virol. Methods* **272**, 113701 (2019).
53. J. M. Ruijter *et al.*, Amplification efficiency: Linking baseline and bias in the analysis of quantitative PCR data. *Nucleic Acids Res.* **37**, e45 (2009).